



Fermi National Accelerator Laboratory

FERMILAB-Conf-98/344

**Particle-Beam Approach to Collective Instabilities—Application to
Space-Charge Dominated Beams**

K. Y. Ng and S. Y. Lee

*Fermi National Accelerator Laboratory
P.O. Box 500, Batavia, Illinois 60510*

November 1998

Published Proceedings of the *16th Advanced ICFA Beam Dynamics Workshop on Nonlinear and Collective Phenomena in Beam Physics*, Arcidosso, Italy, September 1-5, 1998

Disclaimer

This report was prepared as an account of work sponsored by an agency of the United States Government. Neither the United States Government nor any agency thereof, nor any of their employees, makes any warranty, expressed or implied, or assumes any legal liability or responsibility for the accuracy, completeness, or usefulness of any information, apparatus, product, or process disclosed, or represents that its use would not infringe privately owned rights. Reference herein to any specific commercial product, process, or service by trade name, trademark, manufacturer, or otherwise, does not necessarily constitute or imply its endorsement, recommendation, or favoring by the United States Government or any agency thereof. The views and opinions of authors expressed herein do not necessarily state or reflect those of the United States Government or any agency thereof.

Distribution

Approved for public release; further dissemination unlimited.

Copyright Notification

This manuscript has been authored by Universities Research Association, Inc. under contract No. DE-AC02-76CHO3000 with the U.S. Department of Energy. The United States Government and the publisher, by accepting the article for publication, acknowledges that the United States Government retains a nonexclusive, paid-up, irrevocable, worldwide license to publish or reproduce the published form of this manuscript, or allow others to do so, for United States Government Purposes.

Particle-Beam Approach to Collective Instabilities — Application to Space-Charge Dominated Beams

K.Y. Ng

Fermi National Accelerator Laboratory, P.O. Box 500, Batavia, IL 60510*

S.Y. Lee

Physics Department, Indiana University, Bloomington, IN 47405

Abstract. Nonlinear dynamics deals with parametric resonances and diffusion. The phenomena are usually beam-intensity independent and rely on a particle Hamiltonian. Collective instabilities deal with beam coherent motion, where the Vlasov equation is frequently used in conjunction with a beam-intensity dependent Hamiltonian. We address the questions: Are the two descriptions the same? Are collective instabilities the results of encountering parametric resonances whose driving force is intensity dependent? We study here the example of a space-charge dominated beam governed by the Kapchinskij-Vladimirskij (K-V) envelope equation [1]. The stability and instability regions as functions of tune depression and envelope mismatch are compared in the two approaches. The study has been restricted to the simple example of a uniformly focusing channel.

I INTRODUCTION

Traditionally, the thresholds of collective instabilities are obtained by solving the Vlasov equation for collective motion. The modes of instabilities are described by the set of orthonormal eigenfunctions of the characteristic equation and the corresponding complex eigenvalues give the initial growth rates.

The beam dynamics of the Vlasov equation derives from a Hamiltonian that includes wakefields. The unperturbed beam distribution function is computed under the influence of the mean field. The perturbative distribution function is obtained by solving the Vlasov equation, which is often linearized so that the collective eigenmodes can be determined.

The nonlinear Hamiltonian can generally be decomposed into an unperturbed part, H_0 , and a perturbation H_1 . The unperturbed Hamiltonian is derived from the external forces such as the quadrupoles, rf focusing potential, the space-charge mean-field potential, and the potential-well distortion due to low-frequency components of the wakefields.

The perturbation H_1 can arise from nonlinear magnetic fields, high-frequency wakefields, etc. It may have a time-independent component, for example, the

*) Operated by the Universities Research Association, under contracts with the US Department of Energy.

part involving the nonlinear magnetic fields, that gives rise to the dynamical aperture limitation of the dynamical system. On the other hand, it may also have a time-dependent component, which includes the effects of wakefields and produces coherent motion of beam particles. The harmonic content of the wakefields depends on the structure of accelerator components. If one of the resonant frequencies of the wakefields is equal to a fractional multiple of the unperturbed tune of H_0 , including the mean-field potential, a resonance is encountered and coherent particle motion is introduced. This may result in a runaway situation such that collective instability is induced.

Experimental measurements indicate that a small time dependent perturbation can create resonance islands in the longitudinal or transverse phase space and profoundly change the bunch structure [2]. For example, a modulating transverse dipole field close to the synchrotron frequency can split up a well-behaved bunch into beamlets. Although these phenomena are driven by a beam-intensity independent source, they can also be driven by the space-charge force and/or the wakefields of the beam which are intensity dependent. Once perturbed, the new bunch structure can further enhance the wakefields inducing even more perturbation to the circulating beam. Experimental observation of hysteresis in collective beam instabilities seems to indicate that resonance islands have been generated by the wakefields.

For example, the Keil-Schnell criterion [3] of longitudinal microwave instability can be derived from the concept of bunching buckets, or islands, created by the perturbing wakefields. Particles of the beam will execute *synchrotron* motion inside these buckets leading to growth in the momentum spread of the beam. In fact, the collective growth rate is exactly the angular synchrotron frequency inside these buckets. If the momentum spread of the beam is much larger than the bucket height, only a small fraction of the particles in the beam will be affected and collective instabilities will not occur. This mechanism has been called Landau damping.

As a result, we believe that the collective instabilities of a beam can also be tackled from a particle-beam nonlinear dynamics approach, with collective instabilities occurring when the beam particles are either trapped in resonance islands or diffuse away from the beam core because of the existence of a sea of chaos. The advantage of the particle-beam nonlinear dynamics approach is its ability to understand the hysteresis effects and to calculate the beam distribution beyond the threshold condition. Such a procedure may be able to unify our understanding of collective instabilities and nonlinear beam dynamics.

In this work, the stability issues of a space-charge dominated beam in a uniformly focusing channel are considered as an example. In Sect. II, the Hamiltonian formulation of the envelope equation is reviewed. In Sect. III, we present a brief account of the collective-motion approach as studied by Gluckstern, Cheng, Kurennoy, and Ye [4], using the Vlasov equation. For the particle-beam nonlinear dynamic approach, we start with the particle Hamiltonian in Sect. IV, where the particle tune is computed in the presence of beam-envelope oscillations with and without mis-

match. Section V is devoted to parametric resonances, where beam stability is investigated as a function of the space-charge perveance and beam envelope mismatch. In Sec. VI, beam particles having nonzero angular momentum are included. Finally, in Sec. VII, conclusions are given.

II ENVELOPE HAMILTONIAN

First, the envelope Hamiltonian is normalized to unit emittance and unit period. In terms of the normalized and dimensionless envelope radius R , together with its conjugate momentum P , the Hamiltonian for the beam envelope in a uniformly focusing channel can be written as [5,6]

$$H_e = \frac{1}{4\pi} P^2 + V(R) , \quad (2.1)$$

with the potential

$$V(R) = \frac{\mu^2}{4\pi} R^2 - \frac{\mu\kappa}{\pi} \ln \frac{R}{R_0} + \frac{1}{4\pi R^2} , \quad (2.2)$$

where $\mu/(2\pi)$ is the *unperturbed* particle tune, $\kappa = Nr_{\text{cl}}/(\mu\beta^2\gamma^3)$ plays the role of the *normalized* space-charge perveance, N is the number of particles per unit length having the classical radius r_{cl} , and β and γ are the relativistic factors of the beam. The normalized K-V equation then reads

$$\frac{d^2 R}{d\theta^2} + \left(\frac{\mu}{2\pi}\right)^2 R = \frac{2\mu\kappa}{4\pi^2 R} + \frac{1}{4\pi^2 R^3} , \quad (2.3)$$

The radius R_0 of the matched beam envelope or core is determined by the lowest point of the potential; i.e., $V'(R_0) = 0$, or

$$\mu R_0^2 = \sqrt{\kappa^2 + 1} + \kappa = \frac{1}{\sqrt{\kappa^2 + 1} - \kappa} . \quad (2.4)$$

From the second derivative of the potential, the small amplitude tune for envelope oscillations is therefore

$$\nu_e = \frac{2\mu}{2\pi} \left[1 - \kappa \left(\sqrt{\kappa^2 + 1} - \kappa\right)\right]^{1/2} \longrightarrow \begin{cases} 2\frac{\mu}{2\pi} & \kappa \rightarrow 0 \\ \sqrt{2}\frac{\mu}{2\pi} & \kappa \rightarrow \infty \end{cases} \quad (2.5)$$

For a mismatched beam, R varies between R_{min} and R_{max} . To derive the tune of the mismatched envelope, it is best to go to the action-angle variables. The envelope action can be computed from the envelope Hamiltonian via

$$J_e = \frac{1}{2\pi} \oint P dR . \quad (2.6)$$

The envelope tune is then

$$Q_e = \frac{dE_e}{dJ_e} = \nu_e + \alpha_e J_e + \dots, \quad (2.7)$$

where E_e is the Hamiltonian value of the beam envelope, and the detuning α_e , defined by

$$H_e = \nu_e J_e + \frac{1}{2} \alpha_e J_e^2 + \dots, \quad (2.8)$$

is computed to be

$$\alpha_e = \frac{3}{16\pi^3 R_0^4 \nu_e^2} \left(\mu\kappa + \frac{5}{R_0^2} \right) - \frac{5}{48\pi^5 R_0^6 \nu_e^4} \left(\mu\kappa + \frac{3}{R_0^2} \right)^2 + \dots. \quad (2.9)$$

To obtain the envelope tune for large mismatch, one must compute numerically the action integral to obtain

$$Q_e = \frac{dE_e}{dJ_e} = 2\pi \left[\oint \frac{\partial P}{\partial E_e} dR \right]^{-1}, \quad (2.10)$$

The envelope tune is plotted in Fig. 1 as a function of the maximum envelope radius R_{\max} , which for small mismatch is related to the envelope action J_e by

$$R = R_0 + \left(\frac{J_e}{\pi\nu_e} \right)^{1/2} \cos Q_e \theta. \quad (2.11)$$

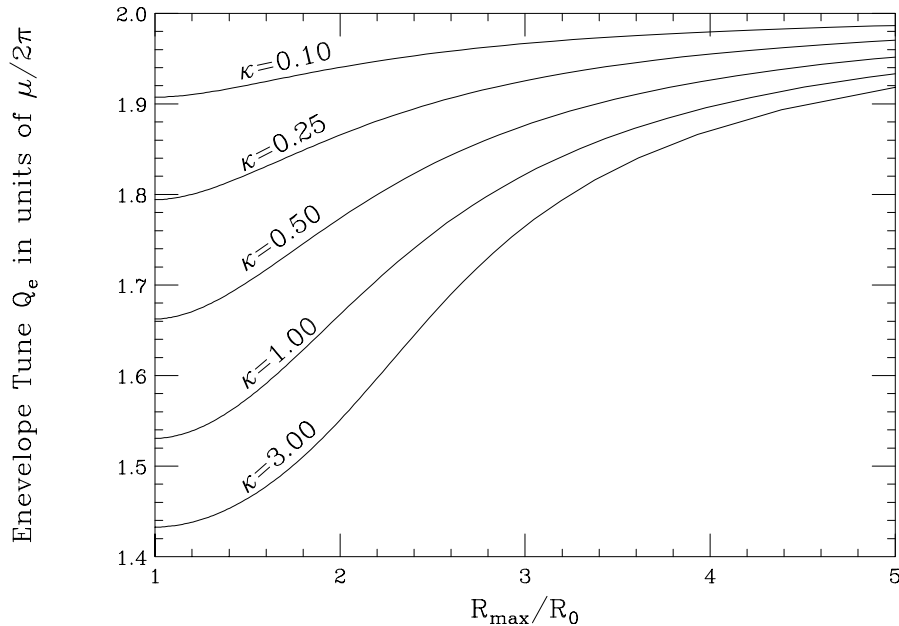


FIGURE 1. Envelope tune Q_e versus envelope mismatch R_{\max}/R_0 for various space-charge perveance κ . Notice that Q_e is represented by ν_e at $R_{\max}/R_0 = 1$ when the beam envelope is matched.

III COLLECTIVE-MOTION APPROACH

Gluckstern, Cheng, Kurennoy, and Ye [4] have studied the collective beam stabilities of a space-charge dominated K-V beam in a uniformly focusing channel. The particle distribution f is separated into the unperturbed distribution f_0 and the perturbation f_1 :

$$f(u, v, \dot{u}, \dot{v}; \theta) = f_0(u^2 + v^2 + \dot{u}^2 + \dot{v}^2) + f_1(u, v, \dot{u}, \dot{v}; \theta), \quad (3.1)$$

where u and v are the normalized transverse coordinates which are functions of the ‘time’ variable θ . Their derivatives with respect to time are denoted by \dot{u} and \dot{v} . The unperturbed distribution

$$f_0(u^2 + v^2 + \dot{u}^2 + \dot{v}^2) = \frac{I_0}{v_0 \pi^2} \delta(u^2 + v^2 + \dot{u}^2 + \dot{v}^2 - 1) \quad (3.2)$$

is the steady-state solution of the K-V equation (2.3) and is therefore time-independent. In the notation of Gluckstern, Cheng, Kurennoy, and Ye, I_0 is the average beam current and v_0 the longitudinal velocity of the beam particles. The perturbed distribution generates an electric potential G , which is given by the Poisson’s equation

$$\nabla^2 G(u, v, \theta) = -\frac{1}{\epsilon_0} \int d\dot{u} \int d\dot{v} f_1(u, v, \dot{u}, \dot{v}; \theta), \quad (3.3)$$

so that the Hill’s equations in the two transverse planes become

$$\ddot{u} + u = -\frac{e\beta}{m_0 v_0^2 \epsilon} \frac{\partial G}{\partial u}, \quad \ddot{v} + v = -\frac{e\beta}{m_0 v_0^2 \epsilon} \frac{\partial G}{\partial v}, \quad (3.4)$$

where ϵ stands for the transverse emittance of the beam and m_0 the rest mass of the beam particle.

For small perturbation, the perturbation distribution is proportional to the derivative of the unperturbed distribution. This enables us to write

$$f_1(u, v, \dot{u}, \dot{v}; \theta) = g(u, v, \dot{u}, \dot{v}; \theta) f_0'(u^2 + v^2 + \dot{u}^2 + \dot{v}^2). \quad (3.5)$$

Substituting into the linearized Vlasov equation, we obtain

$$\frac{\partial g}{\partial \theta} + \dot{u} \frac{\partial g}{\partial u} + \dot{v} \frac{\partial g}{\partial v} - u \frac{\partial g}{\partial \dot{u}} - v \frac{\partial g}{\partial \dot{v}} = \frac{2e\beta}{m_0 v_0^2 \epsilon} \left[\dot{u} \frac{\partial G}{\partial u} + \dot{v} \frac{\partial G}{\partial v} \right]. \quad (3.6)$$

Noting that the potential G is a polynomial, Gluckstern, *et. al.* are able to solve for g and G consistently in terms of hypergeometric functions. Thus a series of orthonormal eigenmodes are obtained for the perturbed distribution with their corresponding eigenfrequencies. These modes are characterized by (j, m) , where j is the radial eigennumber and m the azimuthal eigennumber.

For the azimuthally symmetric modes, $m=0$. The (1,0) is the breathing mode of uniform density at a particular time. The (2,0) mode oscillates with a radial

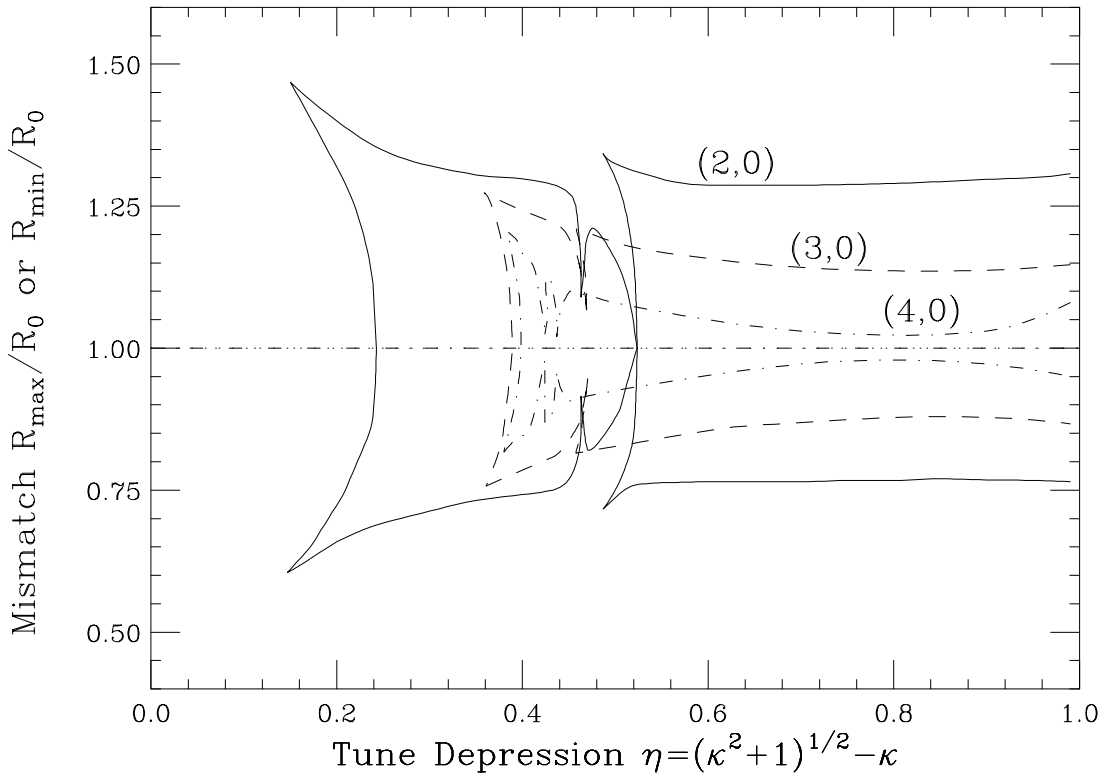


FIGURE 2. Beam stability plot versus particle tune depression η and beam envelope mismatch. The stability region for the (2,0) mode is enclosed by the solid curve, that for the (3,0) mode by the dashed curve, and that for the (4,0) mode by the dot-dashed curve. (Reproduced from Ref. 4).

node between $R = 0$ and $R = R_0$ so that the density becomes nonuniform. The higher modes are similar, with the $(j, 0)$ having $j - 1$ radial nodes. When the eigenfrequency of a mode is complex, the mode becomes unstable with a collective growth rate. Stability is studied in terms of tune depression $\eta = \sqrt{\kappa^2 + 1} - \kappa$ and the amount of envelope mismatch. The former is defined as the ratio of the particle tune with space charge to the particle tune without space charge for a *matched* beam. Thus η ranges from 0 to 1; $\eta = 1$ implies zero space charge while $\eta = 0$ implies infinite space charge.

Gluckstern, *et. al.* showed that the (1,0) mode is stable for any amount of mismatch and tune depression. The (2,0) mode becomes unstable at zero mismatch when the tune depression $\eta < 1/\sqrt{17} = 0.2435$. It is also unstable when the mismatch is large. This is plotted in Fig. 2 with the stable region enclosed by the solid curve, a reproduction of Ref. 4. The stability regions of the (3,0) and (4,0) modes, enclosed by dashes and dot-dashes, respectively, are also shown. These latter two modes become unstable at zero mismatch when the tune depressions are less than 0.3859 and 0.3985, respectively. They found that the modes become more unstable as the number of radial nodes increases. Among all the azimuthals, they also noticed that the azimuthally symmetric modes ($m = 0$) are the most unstable.

IV PARTICLE-BEAM APPROACH

A Particle Hamiltonian

We want to investigate whether the instability regions in the plane of tune depression and mismatch can be explained by nonlinear parametric resonances. First let us study the transverse motion of a particle having zero angular momentum. The situation of finite momentum will be discussed later in Sec. VI. We choose y as the particle's transverse coordinate with canonical angular momentum p_y . Its motion is perturbed by an azimuthally symmetric oscillating beam core of radius R . The particle Hamiltonian is [6]

$$H_p = \frac{1}{4\pi} p_y^2 + \frac{\mu^2}{4\pi} y^2 - \frac{2\mu\kappa}{4\pi R^2} y^2 \Theta(R - |y|) - \frac{2\mu\kappa}{4\pi} \left(1 + 2 \ln \frac{|y|}{R}\right) \Theta(|y| - R) , \quad (4.1)$$

giving the equation of motion for y ,

$$\frac{d^2 y}{d\theta^2} + \left(\frac{\mu}{2\pi}\right)^2 y = \frac{\mu\kappa}{2\pi^2 R^2} y \Theta(R - |y|) + \frac{\mu\kappa}{2\pi^2 |y|} \Theta(|y| - R) . \quad (4.2)$$

For a weakly mismatched beam, the envelope radius can be written as

$$R = R_0 + \Delta R \cos Q_e \theta . \quad (4.3)$$

The particle Hamiltonian can also be expanded in terms of the equilibrium envelope radius R_0 , resulting

$$H_p = H_{p0} + \Delta H_p . \quad (4.4)$$

The unperturbed Hamiltonian is

$$H_{p0} = \frac{1}{4\pi} p_y^2 + \frac{\mu^2}{4\pi} y^2 - \frac{2\mu\kappa}{4\pi R_0^2} y^2 \Theta(R_0 - |y|) - \frac{2\mu\kappa}{4\pi} \left(1 + 2 \ln \frac{|y|}{R_0}\right) \Theta(|y| - R_0) , \quad (4.5)$$

and the perturbation

$$\Delta H_p \approx -\frac{\mu\kappa}{\pi R_0^2} \left[\frac{\Delta R}{R_0} (y^2 - R_0^2) + \frac{3\Delta R^2}{2R_0^2} \left(y^2 - \frac{1}{3}R_0^2\right) + \dots \right] \Theta(R_0 - |y|) . \quad (4.6)$$

Note that many non-contributing terms, like the ones involving the δ -function and δ' -function, have been dropped. Additionally, envelope oscillations do not perturb particle motion outside envelope radius; thus the perturbing potential in Eq. (4.6) exists only inside the envelope.

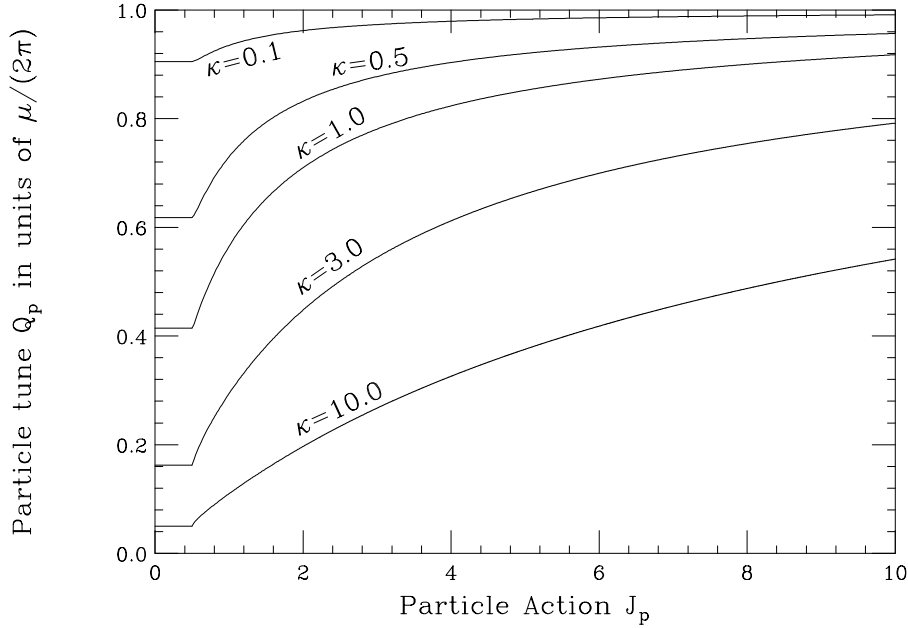


FIGURE 3. Particle tune Q_p as function of particle action J_p and space-charge perveance κ for a matched beam.

For a matched beam, $\Delta H_p = 0$. Inside the core of uniform distribution, the particle motion is linear and its tune can be readily obtained:

$$\nu_p = \frac{\mu}{2\pi} \left(1 - \frac{2\kappa}{\mu R_0^2} \right)^{1/2} = \frac{\mu}{2\pi} \left(\sqrt{\kappa^2 + 1} - \kappa \right) .$$

Thus, $\eta = \sqrt{\kappa^2 + 1} - \kappa$ is the tune depression.

When the particle spends time oscillating outside the beam envelope, its tune has to be computed numerically. First the particle action is defined as

$$J_p = \frac{1}{2\pi} \oint p_y dy . \quad (4.7)$$

The particle tune Q_p is then given by

$$Q_p = \frac{dE_p}{dJ_p} = 2\pi \left[\oint \frac{\partial p_y}{\partial E_p} dy \right]^{-1} , \quad (4.8)$$

where E_p is the Hamiltonian value of the beam particle. The result is shown in Fig. 3 for various space-charge perveance κ . We see that when the particle motion is completely inside the beam envelope ($J_p < \frac{1}{2}$), the particle tune is a constant and is given by ν_p depending on κ only. As the particle spends more and more time outside the beam envelope, its tune increases because the space-charge force decreases as y^{-1} outside the envelope.

B Particle Tune Inside a Mismatched Beam

To simplify the algebra, it is advisable to scale away the unperturbed particle tune $\mu/(2\pi)$ through the transformation:

$$\mu R^2 \longrightarrow R^2, \quad \left(\frac{\mu}{2\pi}\right)\theta \longrightarrow \theta. \quad (4.9)$$

The envelope equation becomes

$$\frac{d^2 R}{d\theta^2} + R = \frac{2\kappa}{R} + \frac{1}{R^3} \quad (4.10)$$

The particle equation is, after the same transformation,

$$\frac{d^2 y}{d\theta^2} + y - \frac{2\kappa}{R^2} y \Theta(R - |y|) - \frac{2\kappa}{y} \Theta(|y| - R) = 0, \quad (4.11)$$

where the replacement $\mu y^2 \rightarrow y^2$ has also been made. For one envelope oscillation period, the envelope radius R is periodic and Eq. (4.11) *inside* the envelope core becomes a Hill's equation with effective *field gradient* $K(\theta) = 1 - 2\kappa/R^2(\theta)$. The solution is then exactly the same as the Floquet transformation by choosing $y = aw(\theta) \cos[\psi(\theta) + \delta]$. It is easy to show that the differential equation for w is exactly the envelope equation of Eq. (4.10). Thus we can replace w by R , and R^2 becomes the effective *betatron function*. Since the particle makes Q_p/Q_e betatron oscillations during one envelope fluctuation period, where Q_p is the particle tune, we have

$$\frac{Q_p}{Q_e} = \frac{\Delta\psi}{2\pi} = \frac{1}{2\pi} \oint \frac{d\theta}{R^2(\theta)}. \quad (4.12)$$

In Floquet's notation, we define $\hat{y} = y/R$. Then Eq. (4.2) describing the motion of a particle modulated by a beam envelope becomes

$$\frac{d^2 \hat{y}}{d\psi^2} + \hat{y} + 2\kappa R^2 \left[\frac{\hat{y}^2 - 1}{\hat{y}} \right] \Theta(|\hat{y}| - 1) = 0. \quad (4.13)$$

Thus, all particles inside the beam envelope have a fixed tune depending on the amount of space charge and envelope mismatch. Particles spending part of the time outside the beam envelope will have larger tunes.

The Floquet transformation can also be accomplished by a canonical transformation employing the generating function

$$F_2(y, \hat{p}_y; \theta) = \frac{y\hat{p}_y}{R(\theta)} + \frac{yR'(\theta)}{2R(\theta)}, \quad (4.14)$$

where the prime denotes derivative with respect to θ . The new Hamiltonian in the Floquet coordinates becomes

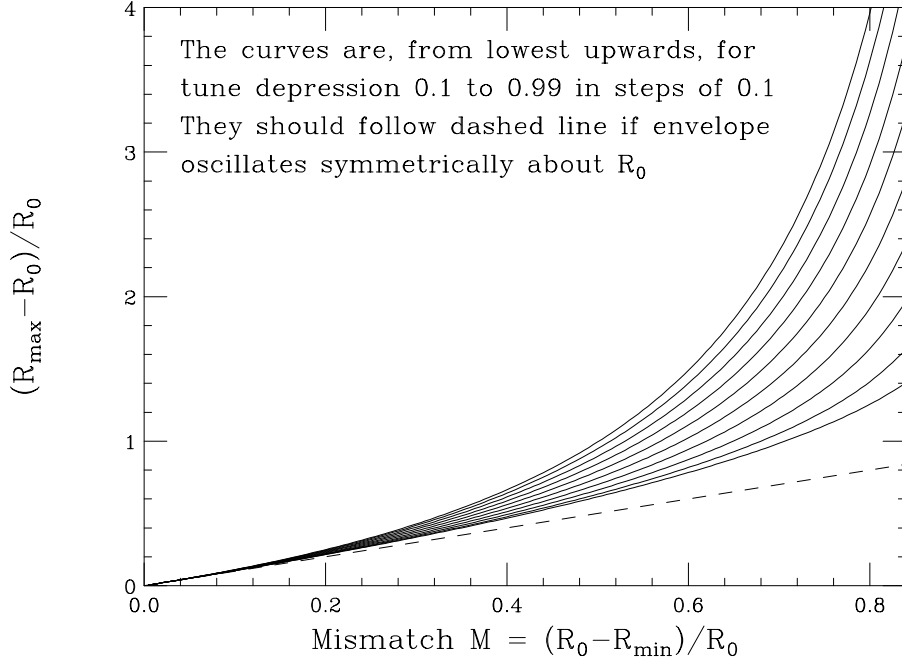


FIGURE 4. Plot of $(R_{\max} - R_0)/R_0$ versus $M = (R_0 - R_{\min})/R_0$ showing that the envelope oscillation is very asymmetric about the equilibrium radius R_0 when both the mismatch and tune depression are large.

$$\hat{H}_p(\hat{y}, \hat{p}_y; \theta) = \frac{1}{R^2(\theta)}(\hat{y}^2 + \hat{p}_y^2) + \kappa(\hat{y}^2 - \ln \hat{y}^2) \Theta(|\hat{y}| - 1) . \quad (4.15)$$

For a small mismatch core fluctuation, we can write $R = R_0(1 - M \cos Q_e \theta)$, where M can be interpreted as the mismatch parameter. The integral in Eq. (4.12) can be performed analytically to give

$$Q_p = \frac{\nu_p}{(1 - M^2)^{3/2}} , \quad (4.16)$$

where $\nu_p = R_0^{-2} = \sqrt{\kappa^2 + 1} - \kappa$, in the presence of the transformation (4.9), is the particle tune when the envelope is matched. The analytic formula of Eq. (4.16), however, is only valid when the mismatch parameter $M \lesssim 0.2$. The reason is that the envelope equation is nonlinear in the presence of space charge. In other words, while minimum envelope radius is given by $R_{\min} = (1 - M)R_0$, the maximum envelope radius is always $R_{\max} > (1 + M)R_0$. In fact, when $M \rightarrow 1$, $R_{\min} \rightarrow 0$, but $R_{\max} \rightarrow \infty$. This can be seen in Fig. 4 when $(R_{\max} - R_0)/R_0$ is plotted against $M = (R_0 - R_{\min})/R_0$. If the envelope oscillations were symmetric about R_0 , the plot would follow the 45° dashed line instead. We see that the deviation is large when the mismatch and tune depression are large. When the approximation $R = R_0(1 - M \cos Q_e \theta)$ breaks down, the particle tune can still be easily evaluated by performing the integral in Eq. (4.12) numerically. Figure 5 shows the deviation of the actual particle tune Q_p from its analytic formula of Eq. (4.16).

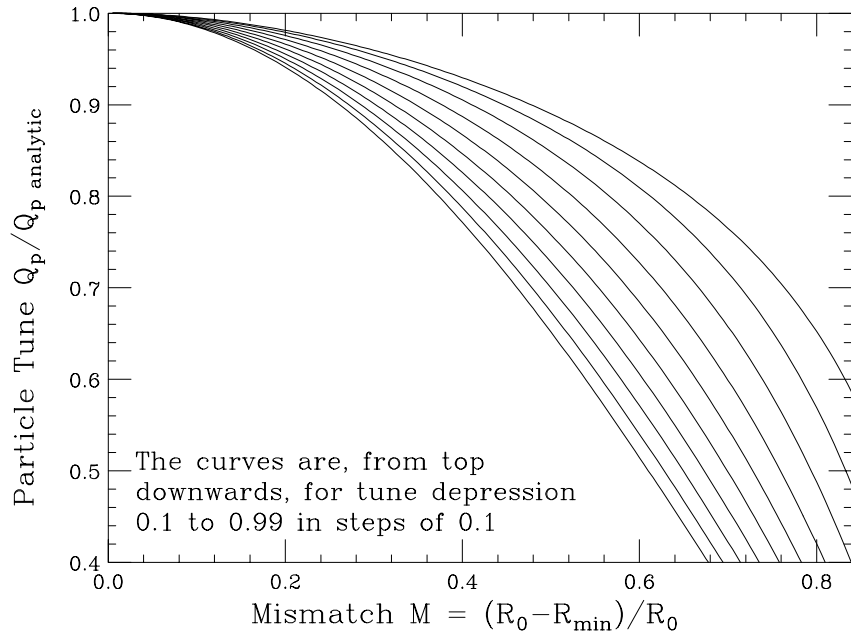


FIGURE 5. Plot showing the deviation of the actual particle tune Q_p from the value of the analytic formula of Eq. (4.16) in the presence of mismatch.

V PARAMETRIC RESONANCES

Particle motion is modulated by the oscillating beam envelope. Therefore, to study the resonance effect, we need to include the perturbation part ΔH_p of the particle Hamiltonian. We expand it as a Fourier series in the angle variable ψ_p yielding, for example,

$$(y^2 - R_0^2) \Theta(R_0 - |y|) = \sum_{n=-\infty}^{\infty} G_n(J_p) e^{in\psi_p} . \quad (5.1)$$

Since ΔH_p is even in y , only even n harmonics survive. The particle Hamiltonian then becomes

$$H_p = H_{p0} + \frac{\mu\kappa}{2\pi R_0^2} \sum_{m=1}^{\infty} \sum_{\substack{n>0 \\ \text{even}}} (m+1) M^m |G_{nm}| \\ \times [\cos(n\psi_p - mQ_e\theta + \gamma_n) + \cos(n\psi_p + mQ_e\theta + \gamma_n)] + \dots \quad (5.2)$$

where γ_n are some phases and use has been made of $R_0 - R = MR_0 \cos Q_e\theta$, the approximation for small mismatch.

Focusing on the $n:m$ resonance, we perform a canonical transformation to the resonance rotating frame (I_p, ϕ_p) to get

$$\langle H_p \rangle = E_p(I_p) - \frac{m}{n} Q_e I_p + h_{nm}(I_p) \cos n\phi_p , \quad (5.3)$$

with the effective κ -dependent resonance strength given by

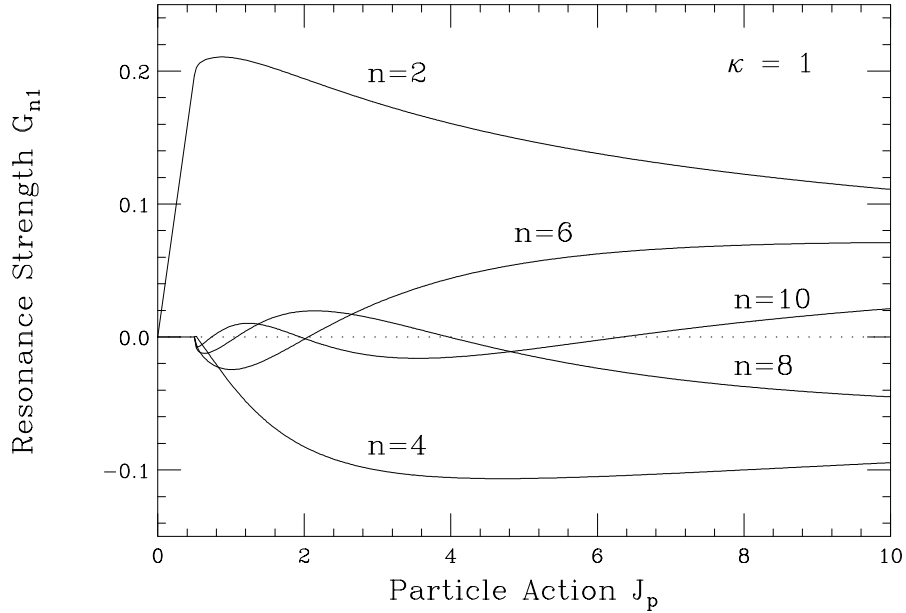


FIGURE 6. Plot of driving strengths of the first-order resonance, G_{n1} , versus the particle action J_p . Inside the envelope ($J_p < \frac{1}{2}$), only G_{21} is nonzero. Once outside the envelope, however, $|G_{n1}|$ for $n \geq 2$ increases rapidly from zero.

$$h_{nm} = \frac{(m+1)M^m \mu \kappa}{2\pi R_0^2} |G_{nm}(I_p)| . \quad (5.4)$$

As usual, there are n stable and n unstable fixed points which can be found easily. Since ΔH_p is a polynomial up to y^2 only and $y \propto \sin \psi_p$, we have, inside the envelope,

$$G_{nm} = \frac{1}{4\pi Q_e} J_p \delta_{n2} , \quad (5.5)$$

implying that only 2: m resonances are possible. Outside the envelope the resonance driving strength can also be computed. These are plotted in Fig. 6. We see that although the driving strengths G_{n1} for $n > 2$ vanish inside the envelope ($J_p < \frac{1}{2}$), they increase rapidly once outside. Including noises of all types, particles inside the K-V beam envelope can leak out. This situation is particularly true when the particle tune is equal to a fractional multiple of the envelope tune. A small perturbation may drive particles outside the beam envelope. Once outside, because of the nonvanishing driving strengths, these particles may be trapped into resonance islands or diffuse into resonances farther away. Once trapped or diffused, these particles cannot wander back into the envelope core to stabilize the core distribution. As more and more envelope particles leak out, this is viewed as an instability.

Our job is, therefore, to map out the location of parametric resonances in the plane of mismatch and tune depression. Because particles are affected only by

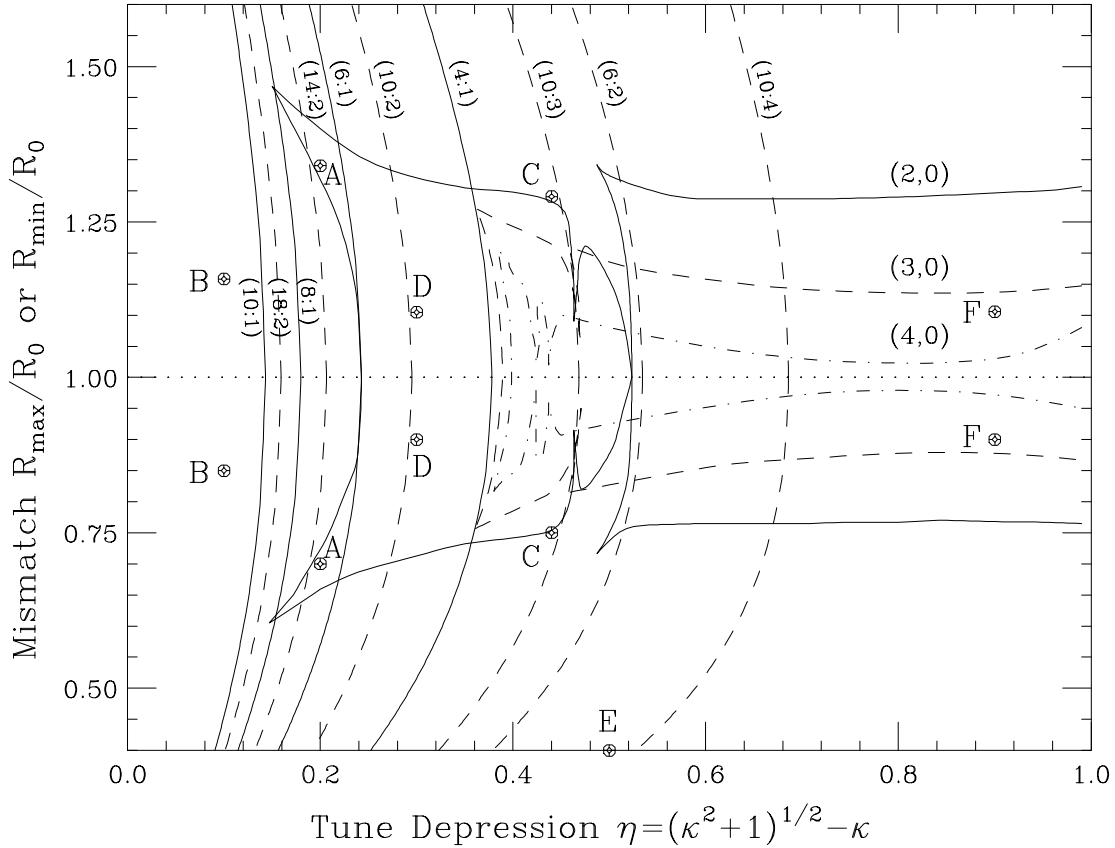


FIGURE 7. Plot of parametric resonance locations in the plane of tune-depression beam envelope mismatch. First-order resonances are shown as solid while second- and higher-order resonances as dashes. Overlaid on top are the instability boundaries of modes (2,0), (3,0), and (4,0) derived by Gluckstern, *et. al.*

resonances when they are just outside the envelope core, their tunes are essentially the tune inside the beam envelope. At zero mismatch, the threshold for the $n:m$ resonance can therefore be derived by equating ν_p/ν_e to m/n . Thus

$$\frac{\nu_p}{\nu_e} = \frac{\sqrt{\kappa^2 + 1} - \kappa}{2 \left[1 - \kappa (\sqrt{\kappa^2 + 1} - \kappa) \right]^{1/2}} \leq \frac{m}{n}, \quad \text{or} \quad \kappa \geq \frac{\left(\frac{n}{m}\right)^2 - 4}{\sqrt{8 \left[\left(\frac{n}{m}\right)^2 - 2 \right]}}. \quad (5.6)$$

In particular, for the 6:1 resonance, $\kappa \geq 8/\sqrt{17} = 1.9403$, or the tune depression is $\eta \leq 1/\sqrt{17} = 0.2425$, which agrees with Gluckstern's instability threshold for the (2,0) excitation.

For a mismatched beam, the threshold for the $n:m$ resonance is obtained by equating Q_p/Q_e at that mismatch to m/n . These resonances are labeled in Fig. 7 in the plane of tune depression and mismatch. The locus of the 2:1 resonance is the vertical line $\eta = 1$. This is obvious, because at zero space charge the particle

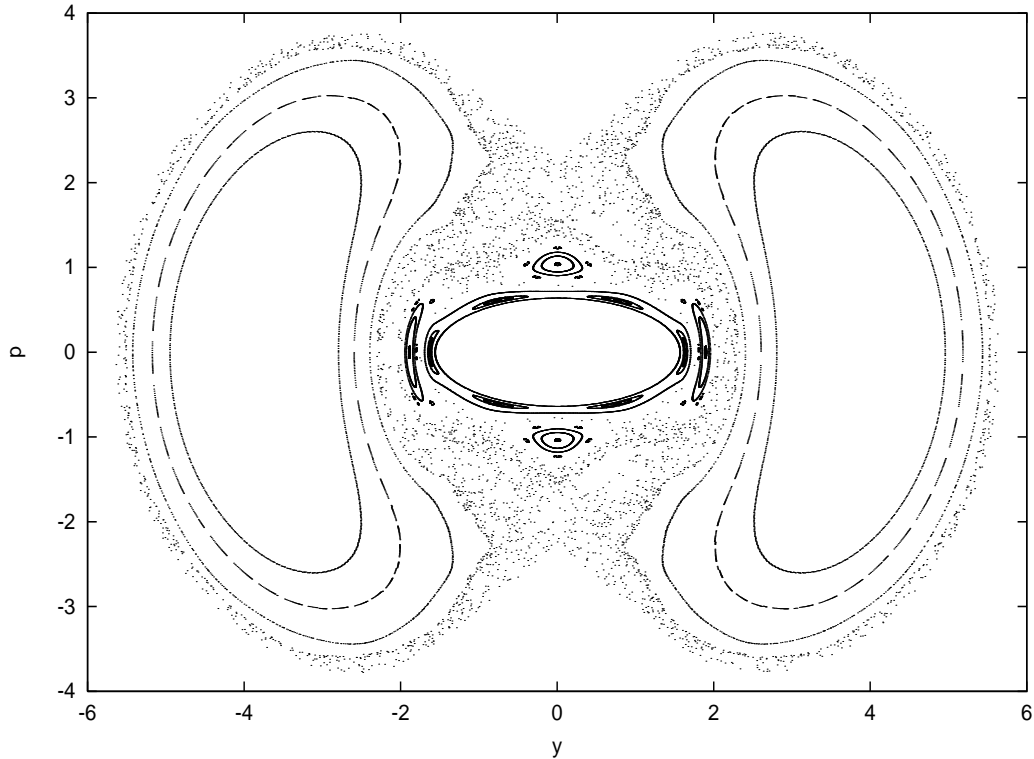


FIGURE 8. Poincaré surface of section in particle phase space (y, p) with $\eta = 0.20$ ($\kappa = 2.4$) and $M = 0.3$ corresponding to Points A in Fig. 7.

tune is exactly two times the envelope tune regardless of mismatch. Also, it is clear from Eq. (4.13) that there will not be any Mathieu instability or half-integer stop-band. Thus it appears that the 2:1 resonance would not influence the stability of a space-charge dominated beam. This is, in fact, not true. The stable fixed points of the 2:1 resonance are usually far away from the beam envelope. Thus particles can diffuse towards the 2:1 resonance to form the halo of the beam. As more and more particles diffuse from the beam core into the 2:1 resonance, the beam becomes unstable.

Trackings have been performed for particles outside the envelope core using the fourth-order symplectic integrator developed by Forest and Berz [7]. The Poincaré surface of section is shown in Fig. 8 for the situation $\eta = 0.20$ ($\kappa = 2.4$) and $M = 0.3$. This corresponds to Points A in Fig. 7. The innermost torus is the beam envelope. The sections are taken every envelope oscillation period when the envelope radius is at a minimum. For each envelope oscillation period, 500 to more than 1000 time steps have been used. We see that as soon as particles diffuse outside the beam envelope, they will encounter the 6:1 resonance, which is bounded by tori. This explains the front stability boundary of the (2,0) mode of Gluckstern, *et. al.* Since the 4:1 resonance is a strong one, its locus explains the front stability boundaries of Gluckstern's (3,0) and (4,0) modes also.

The Poincaré surface of section corresponding to Points B of Fig. 7 with $\eta = 0.10$ ($\kappa = 4.95$) $M = 0.15$ is shown in Fig. 9. This is a close-up view showing only the

region near the beam envelope; the 2:1 resonance and its separatrices are not shown because they look similar to those depicted in Fig. 8. We see resonances like 14:2, 8:1, 16:2, 9:1, 10:1, etc, which are so closely spaced that they overlap to form a chaotic region. Particles that diffuse outward from the beam envelope will wander easily towards the 2:1 resonance along its separatrix. This region, where $\eta \lesssim 0.2$, is therefore very unstable.

Figure 10 shows the close-up Poincaré surface of section of Points C in Fig. 7 with $\eta = 0.44$ ($\kappa = 0.916$) and $M = 0.25$. Here the particles see many parametric resonances when they are outside the beam envelope; first the 10:3, followed by the 6:2, 8:3, 10:4, and then a chaotic layer going towards the 2:1 resonance. The resonances are separated by good tori and the instability growth rate should be small. Thus, this is the region on the edge of instability.

On the other hand, the Poincaré surface of section in Fig. 11 corresponding to Points D of Fig. 7 with $\eta = 0.30$ ($\kappa = 1.517$) and $M = 0.10$ shows the 6:2 resonance well separated from the 10:4 resonance with a wide area of good tori. Also the width of the 10:4 resonance is extremely narrow so that particles can hardly be trapped there. Unlike the situation in Figs. 9 and 10, there is no chaotic region at the unstable fixed points and inner separatrices of the 2:1 resonance, making diffusion towards this resonance impossible. This region will be relatively stable.

Next let us consider the region with very large beam envelope mismatch like Points E of Fig. 7 with $\eta = 0.50$ ($\kappa = 0.75$) and $M = 0.60$. (The other Point E is at $R_{\max}/R_0 = 2.067$ and is therefore not visible in Fig. 7). The close-up Poincaré surface of section in Fig. 12 shows the beam envelope radius at $y = 0.566$ when $p_y = 0$. We can see that the unstable fixed points and the inner separatrices of 2:1 resonance are very close by and are very chaotic. As soon as a particle diffuses out to $y = 0.62$, it reaches the chaotic sea and wanders towards the 2:1 resonance. Because the chaotic region is so close to the beam envelope, this region of large mismatch is also unstable. As a result, we can interpret Gluckstern's region of instability at large mismatch as chaotic region leading to the 2:1 resonance being too close to the beam envelope.

Finally, we look at Points F of Fig. 7, which have small space charge $\kappa = 0.0106$ or $\eta = 0.90$ and small mismatch $M = 0.10$. The Poincaré surface of section is shown in Fig. 13. The beam envelope is surrounded by good tori far away from the separatrices of the 2:1 resonance and no parametric resonances are seen. This is evident also from Fig. 7 that this region is not only free from primary resonances but also many higher-order resonances. The unstable fixed points and the separatrices of the 2:1 resonance are well-behaved and not chaotic. Thus these points are very stable. If we keep the same space-charge perveance and increase the amount of envelope mismatch, we also do not see in the Poincaré surface of section any parametric resonances between the beam envelope and the separatrices for the 2:1 resonance. However, although the separatrices of the 2:1 resonance are not chaotic, they become closer and closer to the beam envelope. When the separatrices are too close, particles that are driven by a small perturbation away from the beam envelope will have a chance of traveling along the separatrices of

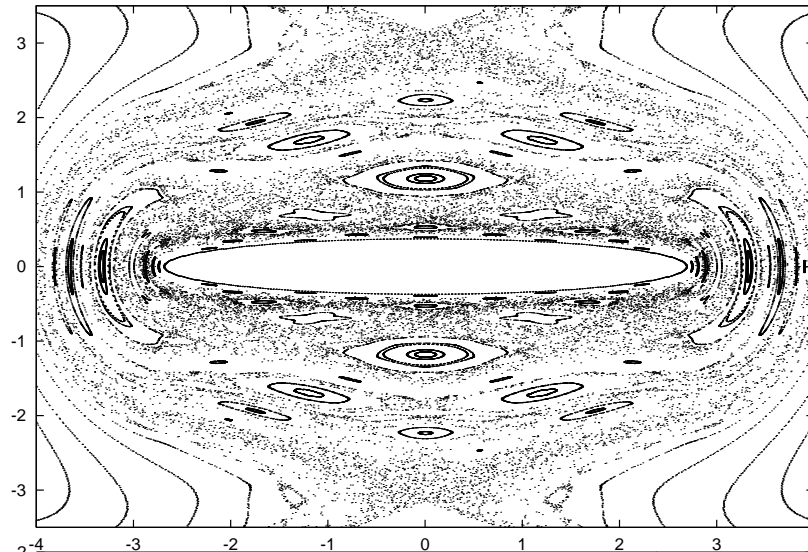


FIGURE 9. $\eta = 0.10$
 $(\kappa = 4.95)$ $M = 0.15$,
 for Points B in Fig. 7.

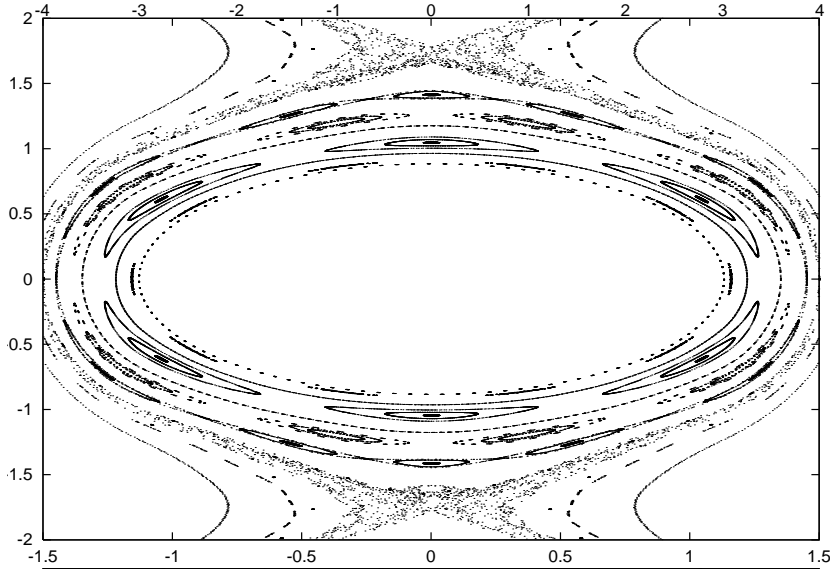


FIGURE 10. $\eta = 0.44$
 $(\kappa = 9.16)$ $M = 0.25$,
 for Points C in Fig. 7.

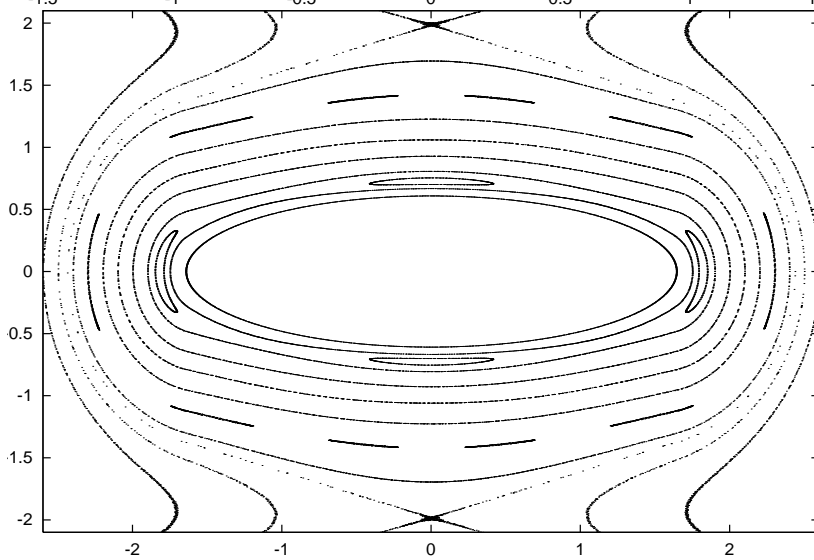


FIGURE 11. $\eta = 0.30$
 $(\kappa = 1.517)$ $M = 0.10$,
 for Points D in Fig. 7.

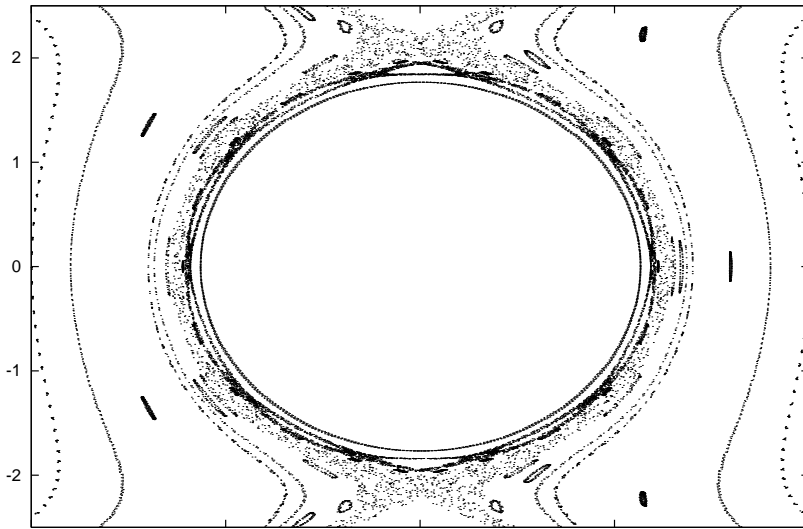


FIGURE 12. $\eta = 0.50$
 $(\kappa = 0.75)$ $M = 0.60$,
 for Points E in Fig. 7.

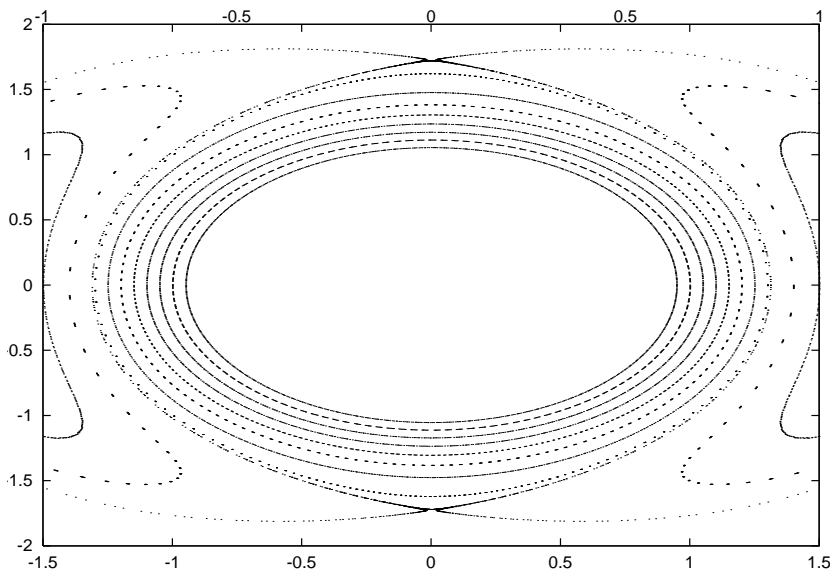


FIGURE 13. $\eta = 0.90$
 $(\kappa = 0.1056)$ $M = 0.10$,
 for Points F in Fig. 7.

the 2:1 resonance to form beam halo. From our discussions above, it is clear that to avoid instability and halo formation, the beam should have small mismatch and be in a region that is far away from parametric resonances in the plane of mismatch and tune depression. The best solution for stability is certainly when the beam has small mismatch and small space-charge perveance.

The deep fissures of the (2,0) mode near $\eta = 4.7$ and 5.3 are probably the result of encountering the 10:3 and 6:2 parametric resonances. The width of the fissures should be related to the width of the resonance islands, which can be computed in the standard way. In general, a lower-order resonance island, like the 4:1, is much wider than a higher-order resonance island, like the 6:1.

We tried very hard to examine the region between the 4:1 and 10:3 resonances with a moderate amount of mismatch. We found this region very stable unless it is close to the 10:3 resonance. We could not, however, reproduce the slits that appear in Gluckstern's (4,0) mode.

VI ANGULAR MOMENTUM

Most K-V particles have nonzero angular momentum. When angular momentum is included in the discussion, we first extend the particle Hamiltonian of Eq. (4.15) in Floquet notations to both the x and y transverse planes:

$$\hat{H}_p = \frac{1}{2R^2}(\hat{x}^2 + \hat{y}^2 + \hat{p}_x^2 + \hat{p}_y^2) + \kappa[\hat{x}^2 + \hat{y}^2 - \ln(\hat{x}^2 + \hat{y}^2)]\Theta(\hat{x}^2 + \hat{y}^2 - 1). \quad (6.1)$$

It is preferable to use the circular coordinates (\hat{r}, φ) as independent variables; their canonical momenta are, respectively, \hat{p}_r and \hat{p}_φ . The particle Hamiltonian becomes

$$\hat{H}_p = \frac{1}{2R^2} \left(\hat{r}^2 + \hat{p}_r^2 + \frac{\hat{p}_\varphi^2}{\hat{r}^2} \right) + \kappa(\hat{r}^2 - \ln \hat{r}^2)\Theta(\hat{r} - 1), \quad (6.2)$$

where $\hat{r}^2 = \hat{x}^2 + \hat{y}^2$ and

$$\begin{pmatrix} \hat{p}_r \\ \frac{\hat{p}_\varphi}{\hat{r}} \end{pmatrix} = \begin{pmatrix} \cos \varphi & \sin \varphi \\ -\sin \varphi & \cos \varphi \end{pmatrix} \begin{pmatrix} \hat{p}_x \\ \hat{p}_y \end{pmatrix}. \quad (6.3)$$

Extending the generating function in Eq. (4.14) to include the x coordinates, it is straightforward to show

$$r = R\hat{r} \quad \text{and} \quad \hat{p}_\varphi = \hat{x}\hat{p}_y - \hat{y}\hat{p}_x = xp_y - yp_x. \quad (6.4)$$

Thus \hat{p}_φ is the angular momentum of the particle, which is a constant of motion. Since it has the same functional form in both coordinate systems, its overhead accent $\hat{}$ will no longer be necessary. Particles belonging to the unperturbed K-V distribution are therefore subjected to the restriction

$$\hat{r}^2 + \hat{p}_r^2 + \frac{\hat{p}_\varphi^2}{\hat{r}^2} = 1, \quad (6.5)$$

from which we obtain

$$\hat{r}^2 = \frac{1 - \hat{p}_r^2}{2} + \left[\left(\frac{1 - \hat{p}_r^2}{2} \right)^2 - \hat{p}_\varphi^2 \right]^{1/2}. \quad (6.6)$$

Thus a K-V particle has an angular momentum restricted by

$$|p_\varphi| \leq \frac{|1 - \hat{p}_r^2|}{2} \leq \frac{1}{2}, \quad (6.7)$$

which agrees with the result of Riabko [6] that $2J_r + |p_\varphi| = \frac{1}{2}$, where J_r is the radial action. The equation of motion for the particle radial position inside the beam core is

$$\frac{d^2 \hat{r}}{d\psi^2} + \hat{r} - \frac{p_\varphi^2}{\hat{r}^3} = 0, \quad (6.8)$$

where the Floquet phase advance $d\psi = d\theta/R^2$ has been used. Notice that this is exactly the same as the envelope equation in Eq (4.10) with $\kappa = 0$. We proved in Sec. II that the envelope tune is exactly twice the particle tune when $\kappa \rightarrow 0$. Hence, comparing with the equation of motion of a zero-angular-momentum particle in the presence of a mismatched space-charge dominated beam, i.e., Eq. (4.13), we can conclude that the particle radial tune inside the beam core is exactly twice the zero-angular-momentum particle tune for any space charge and mismatch.

Simulations have been performed for the time evolution of the radial motion of a beam particle and then compared with the time evolution of the transverse motion of a particle with zero momentum. One of the simulations is shown in the upper plot of Fig. 14. The particle is a K-V particle with angular momentum $p_\varphi = 0.3$ satisfying the K-V restriction of Eq. (6.6) in a mismatched beam envelope with $M = 0.30$ having a tune depression of $\eta = 0.23$. We see that the shape of oscillations of r shown as solid is very similar to that of y with zero angular momentum shown as dashes. Since r does not go negative, its tune appears to be twice the tune of a zero angular-momentum particle. This plot was performed near a 6:1 resonance for a zero angular-momentum particle and it therefore translates into a 3:1 resonance for a nonzero angular-momentum particle.

It is interesting to point out that as $|p_\varphi| \rightarrow \frac{1}{2}$, the humps that exhibit in the time evolution of the radial motion become more pronounced and time evolution eventually becomes proportional to the envelope oscillation, as is demonstrated in lower plot of Fig. 14. Now the radial tune appears to change suddenly to the envelope tune instead. In fact, this is easy to understand. The equation of motion for the particle radial position is

$$r'' + r = \frac{2\kappa}{R^2}r + \frac{p_\varphi}{r^3}. \quad (6.9)$$

Comparing with the envelope equation (4.10), it is evident that $r = \sqrt{|p_\varphi|}R$ is a solution. Of course, in the Floquet representation, Eq. (6.8) also reflects such a solution. Thus, we come across an ambiguity that the radial tune can assume two different values. This ambiguity can be resolved by investigating the Poincaré surface of section of the radial motion. In the Floquet coordinates, the trajectory is represented by one point, $\hat{r} = \sqrt{|p_\varphi|}$ and $\hat{p}_r = 0$. In the (r, p_r) coordinates, the Poincaré surface of section is also a single point since the phase-space position of the particle is plotted only every envelope period. In fact, from Eq. (6.2), the Hamiltonian in the Floquet representation, it is clear that the solution $\hat{r} = \sqrt{|p_\varphi|}$ is the lowest point of the radial potential. This is the equilibrium solution which, in the case of a Hill's equation, is equivalent to a particle traveling along an orbit passing through the centers of all elements. Therefore, even in this solution, the radial tune is *not* equal to the envelope tune, but remains twice the tune in the Cartesian coordinates.

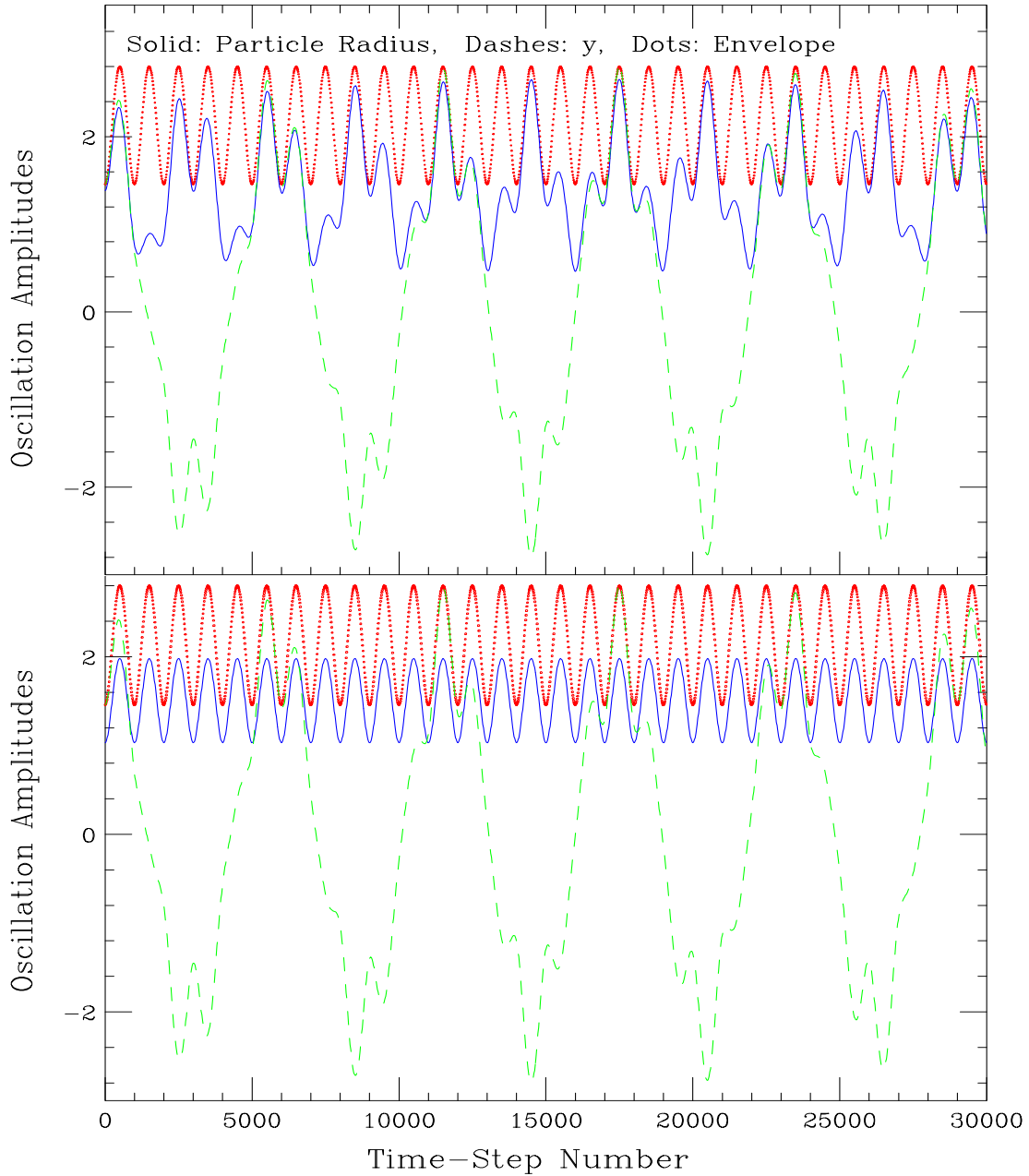


FIGURE 14. Plots showing the time evolution of the radial position r of a K-V particle in solid with nonzero angular momentum inside a beam envelope with mismatch $M = 0.30$ and space-charge perveance $\kappa = 2.059$ ($\eta = 0.23$). The time evolution y of a zero-angular-momentum particle is also shown in dashes. The simulation has been performed at the 6:1 resonance for the zero-angular-momentum particle. In the top plot, the radial motion has an angular momentum of $p_\varphi = 0.30$. The radial oscillation is two times as fast as that of the particle with zero angular momentum. In the lower plot, the angular momentum has been increased to $p_\varphi = 0.50$. Now the particle radius r is related to the envelope radius R by $r = \sqrt{|p_\varphi|}R = R/\sqrt{2}$, giving a false impression that the radial tune becomes equal to the envelope tune.

Because of the above discussion, all the $n:m$ parametric resonances that we studied in Sec. V just translate into the $\frac{n}{2}:m$ resonances in a $r-p_r$ Poincaré surface of section. As a result, the stability investigation in the previous section should hold even when particles with finite angular momentum are included.

VII CONCLUSIONS

(a) Collective instabilities of a K-V beam in a uniformly focusing channel have been explained using the particle-beam nonlinear-dynamics approach. First, the loci of the first- and higher-order parametric resonances were mapped in the plane of tune depression and beam envelope mismatch. Different regions in this plane were discussed in terms of their potential for unstable motion. Because the K-V equation is far from realistic, and because of the existence of noises of all types in the accelerators (as well as in the numerical simulations), some particles will diffuse away from the K-V distribution. If the beam envelope ellipse is bounded by invariant tori, and if the diffusion rate is small, the beam will eventually reach equilibrium and we consider this situation stable.

When the particle tune is equal to some fractional multiples of the envelope tune, particle motion encounters parametric resonances in the presence of the space-charge force. As shown in Fig. 6, the resonance strengths for K-V particle are zero inside the beam envelope. However, if the diffusion process is included, the resonance strengths seen by the K-V particles become nonzero and even large as soon as the particles diffuse outside the beam envelope. These particles can move along the separatrices of the parametric resonances, and eventually escape from the K-V core.

As particles escape from the K-V core, density fluctuations will occur in the K-V core. Furthermore, this may enhance the envelope oscillations, driving more particles to the outside of the K-V core. Such a process can induce collective beam instabilities.

It may happen that the island chains outside the beam envelope are so close together that they overlap to form a chaotic sea. In the case where the last invariant torus breaks up, particles leaking out diffuse towards the 2:1 resonance, which is usually much farther away from the beam envelope. These particles form a beam halo. As particles escape from the beam envelope, the beam intensity inside the envelope becomes smaller and the equilibrium radius of the beam core shrinks. Thus more particles will find themselves outside the envelope radius. As this process continues, the beam eventually becomes unstable.

Another severe instability occurs when the envelope mismatch is large even though the space-charge perveance is moderate. In this case, high-order parametric resonances exist near beam envelope. Since the slope of the tune versus the particle action is small, high-order resonances overlap causing more local chaos. Also the unstable fixed points of the 2:1 resonance are nearby. Particles can diffuse easily from the beam envelope towards the 2:1 resonance and again become halo

particles.

It appears that the particle beam will be most stable when the beam envelope is far from parametric resonances. Obviously, this occurs when the space-charge perveance and envelope mismatch are both small.

(b) We see that the regions of stability and instability are similar to but not exactly the same as the results of Gluckstern, *et. al.* There can be many reasons:

1. Only particles outside the envelope core encounter parametric resonances. So far we have been using particle tune Q_p *inside* the envelope core. The tune outside the core is larger. This may produce more curvature of the resonance loci in Fig. 7.
2. Gluckstern, *et. al.* introduced an envelope tune that depends on the space-charge perveance κ only, but is independent of the amount of envelope mismatch. We used an envelope tune that varies with the amount of mismatch.
3. To the lowest order, the Vlasov equation studied by Gluckstern, *et. al.* does involve the perturbation force induced by the perturbation distribution, f_1 , or Poisson's equation of (3.3). In our nonlinear dynamics approach, the particle that escapes from the beam envelope core, always sees the Coulomb force of the *entire unperturbed beam core*, independent of any variation of the core distribution due to the leakage of particles. This is a shortcoming in our approach, which we need to improve in the future.
4. Although the results of Gluckstern, *et. al.* had been checked by simulations using a particle-in-cell code, we suspect the simulations do not have sufficient precision. For example, in one envelope period, the code [8] uses only 100 time steps and only first-order symplectic tracking. In our simulations, we used a fourth-order symplectic integrator [7], and found that at least 500 and sometimes more than 1000 time steps are required in many circumstances. Also, the projections of the perturbed distribution onto the various excitation modes exhibit large fluctuations. Therefore, the growth rates as evaluated might not have been accurate.

(c) The reason that the perturbative force induced by the perturbation distribution has not been included in our discussion is mainly due to the fact that we have been using the envelope Hamiltonian and the particle Hamiltonian separately. This leads to a dependency of the particle equation of motion on the envelope radius, but not the dependency of the equation of motion of the envelope radius on the particle motion. We believe that this is also the reason why we have not been able to compute the growth rates of instabilities.

(d) It is possible that many collective instabilities can be explained by the particle-beam nonlinear dynamics approach. The wakefields of the beam interacting with the particle distribution produce parametric resonances and chaotic regions. Collective instabilities will be the result of particles trapped inside these resonance islands. The perturbed bunch structure further enhances the wakefields to induce these collective particle instabilities.

REFERENCES

1. I.M. Kapchinskij and V.V. Vladimirkij, *Proceedings of the International Conf. on High Energy Accelerators*, p. 274 (CERN, Geneva, 1959).
2. D.D. Caussyn, *et. al.*, Phys. Rev. **A46**, 7942 (1992); M. Ellison, *et. al.*, Phys. Rev. Lett. **70**, 591 (1993); M. Syphers, *et. al.*, Phys. Rev. Lett. **71**, 720 (1993); D. li *et. al.*, Phys. Rev. **E48**, R1638 (1993); D. li *et. al.*, Phys. Rev. **E48**, 3 (1993); H. Huang *et. al.*, Phys. Rev. **E48**, 4678 (1993); Y. Wang *et. al.*, Phys. Rev. **E49**, 1610 (1994); Y. Wang *et. al.*, Phys. Rev. **E49**, 5697 (1994); S.Y. Lee *et. al.*, Phys. Rev. **E49**, 5717 (1994); M. Ellison *et. al.*, Phys. Rev. **E50**, 4051 (1994); L.Y. Liu *et. al.*, Phys. Rev. **E50**, R3344 (1994); D. Li *et. al.*, Nucl Inst. Methods **A 364**, 205 (1995).
3. E. Keil and W. Schnell, CERN Report SI/BR/72-5, 1972; D. Boussard, CERN Report Lab II/RF/Int./75-2, 1975.
4. R.L. Gluckstern, W.-H. Cheng, and H. Ye, Phys. Rev. Lett. **75**, 2835 (1995); R.L. Gluckstern, W.-H. Cheng, S.S. Kurennoy, and H. Ye, Phys. Rev. **E54**, 6788 (1996).
5. S.Y. Lee and A. Riabko, Phys. Rev. **E51**, 1609 (1995).
6. A. Riabko, M. Ellison, X. Kang, S.Y. Lee, D. Li, J.Y. Liu, X. Pei, and L. Wang, Phys. Rev. **E51**, 3529 (1995).
7. E. Forest and M. Berz, LBL Report LBL-25609, ESG-46, 1989.
8. S.S. Kurennoy, private communication.